Comparison of Turbulence Models for Numerical Calculation of Airflow in an annex 20 Room

Author: M.Sc. Lars Køllgaard Voigt

International Centre for Indoor Environment and Energy
Department of Energy Engineering
Technical University of Denmark, DTU
ET-AFM 2000-01
ISBN 87-7475-225-1

Preface

This report is a part of my work as a Ph.D student at the International Centre for Indoor Environment and Energy (ICIE), Department of Energy Engineering, Technical University of Denmark (DTU).

First of all I would like to thank my supervisors Associate Professor Jens Nørkær Sørensen, Department of Energy Engineering, Head of the Fluid Mechanics Section, DTU (principal supervisor), Professor Peter V. Nielsen, Department of Building Technology and Structural Engineering, University of Ålborg and Associate Professor Arsen Melikov, ICIE.

I thank Research Assistant Dan Nørtoft Sørensen, ICIE, who has developed the grid and carried out the final version of the computations.

I would also like to thank Professor Poul Scheel Larsen, Head of the Department of Energy Engineering, DTU, for his help and inspiration in connection with the theoretical chapters in this report. I thank Professor Povl Ole Fanger, Head of the research programme of the ICIE for his advice during preparation of this first part of my Ph.D. study. Finally, I thank my colleagues at the Department of Energy Engineering for the open and social atmosphere in which many interesting discussions have already taken place.

This work has been supported by the Danish Research Council (STVF) as a part of the research programme of the ICIE established at DTU for the period 1998-2007.

Lyngby d. 5/1-2000

Lars Peter Køllgaard Voigt
Department of Energy Engineering
Technical University of Denmark
Building 404/026
DK-2800 Lyngby
E-mail: lkv@et.dtu.dk

Abstract

The report deals with 2-D numerical calculation of room airflow in an isothermal annex 20 room. The report documents the ability of the flow solver *EllipSys2D* to give results in good agreement with measurements for the specified test case. The flow solver is a finite volume code solving the Reynolds Averaged Navier Stokes equations.

Five two-equation turbulence models were tested. These are the standard $k-\epsilon$ model, the low-Reynolds number $k-\epsilon$ model by Launder & Sharma, the $k-\omega$ model by Wilcox, the $k-\omega$ baseline (BSL) model by Menter and the $k-\omega$ Shear Stress Transport (SST) model by Menter.

Except from the $k-\omega$ SST model by Menter, all the models lead to velocity distributions that are in good agreement with measurements. The poor performance of the $k-\omega$ SST model by Menter for the given flow can possibly be explained from the limiter applied to the eddy viscosity.

Applying theory for a two-dimensional wall jet, measurements are compared with calculated values of the turbulent kinetic energy.

Contents

Notation

a_1	Constant in $k-\omega$ SST model	$[\ -\ ]$
$C_\mu, C_{\epsilon 1}, C_{\epsilon 2}$	Empirical constants	$[\ -\ ]$
$\mathcal{D}_k$	Diffusion of k	$[\ \frac{m^2}{s^3}\ ]$
$\mathcal{D}_v$	Viscous diffusion of ϵ	$[\ \frac{m^2}{s^4}\ ]$
$\mathcal{D}_\epsilon$	Turbulent diffusion of ϵ	$[\ \frac{m^2}{s^4}\ ]$
f_μ, f_1, f_2	Viscous damping function	$[\ -\ ]$
k	Turbulent kinetic energy	$[\ \frac{m^2}{s^2}\ ]$
l	Turbulent length scale	$[\ m\ ]$
p	Pressure	$[\ Pa\ ]$
P	Mean pressure	$[\ Pa\ ]$
p'	Fluctuating part of pressure	$[\ Pa\ ]$
$\mathcal{P}_k$	Production of k	$[\ \frac{m^2}{s^3}\ ]$
$\mathcal{P}_\epsilon$	Production of ϵ	$[\ \frac{m^2}{s^4}\ ]$
Tu	Turbulence intensity	$[\ \%\ ]$
u_i	Velocity	$[\ \frac{m}{s}\ ]$
U_i	Mean velocity	$[\ \frac{m}{s}\ ]$
u_i'	Fluctuating part of velocity	$[\ \frac{m}{s}\ ]$
$\mathcal{V}_k$	Effect of molecular viscosity	$[\ \frac{m^2}{s^3}\ ]$
y^+	Sublayer scaled distance to the wall	$[\ -\ ]$
Δy	Distance to the nearest point from the wall	$[\ m\ ]$
β^*, β_1, β_2	Constants in $k-\omega$ model	$[\ -\ ]$
δ_{ij}	Kronecker delta	$[\ -\ ]$
ϵ	Dissipation of turbulent kinetic energy	$[\ \frac{m^2}{s^3}\ ]$
Φ_ϵ	Dissipation of ϵ	$[\ \frac{m^2}{s^4}\ ]$
γ_1, γ_2	Constants in $k-\omega$ model	$[\ -\ ]$
κ	von Karman constant	$[\ -\ ]$
ν	Kinematic viscosity	$[\ \frac{m^2}{s}\ ]$
ν_t	Eddy viscosity	$[\ \frac{m^2}{s}\ ]$
ω	Specific dissipation rate	$[\ \frac{1}{s}\ ]$
ρ	Density	$[\ \frac{kg}{m^3}\ ]$
σ_k	Turbulent Prandtl number in transport equation for k	$[\ -\ ]$
σ_ϵ	Turbulent Prandtl number in transport equation for ϵ	$[\ -\ ]$
$\sigma_{\omega 1}$,$\sigma_{\omega 2}$	Turbulent Prandtl numbers in transport equation for ω	$[\ -\ ]$

Subscripts

0	At inlet condition

Chapter 1

Introduction

The flow in empty ventilated rooms has been studied both experimentally and numerically. Experiments were carried out in 1978 by Nielsen *et al* [11]. In 1990 one of the experimental setups was used as a standard configuration for validation of numerical codes, Nielsen [9]. The codes used to reproduce these experiments are often based on the solution of the time-averaged Navier-Stokes equations. Different ways of modelling turbulence exist, however most interest has been given to two equation models such as the low Reynolds number $k-\epsilon$ model by Launder & Sharma [3], and the $k-\omega$ models by Wilcox [21] and Menter [5]. In this report we concentrate on these models.

The aim of this report is to give a general introduction to turbulence modelling related to room air movement. The transport equation for turbulent kinetic energy k and the dissipation of turbulent kinetic energy ϵ are derived from the Navier-Stokes equation. Furthermore the report documents the ability of the in-house developed flow solver *EllipSys2D* to adequately predict the velocity distribution for the specified test case. Applying theory for a two-dimensional wall jet, measurements of the turbulent kinetic energy are compared with calculated results. It is a matter of course, that the best agreement is found in the wall jet. The *EllipSys2D* flow solver is a finite volume multigrid Navier-Stokes solver, which uses a block structured grid in a non-staggered arrangement. The development of this code was initiated in the beginning of the 90ties by Michelsen [8]. So far the work with *EllipSys2D* has mostly concentrated on external flow, e.g. Sørensen [18].

The test case is the well known two-dimensional isothermal annex 20 room. We test the performance of five different turbulence models, two different $k-\epsilon$ turbulence models, a low-Reynolds number model by Launder & Sharma, [3] in which the transport equations for the turbulent quantities are integrated to the walls, and the standard model using wall laws. For both models acceptable numerical results are obtained. Furthermore, we apply the $k-\omega$ model by Wilcox [21], in which the turbulent quantity ϵ is replaced by the specific dissipation rate ω. We also introduce two zonal versions of the $k-\omega$ model, the baseline model and the shear stress transport model, both by Menter [5]. The former is designed to avoid strong dependency of the arbitrary freestream values, i.e.

ω. In the latter the eddy viscosity is further redefined to account for transport of principal turbulent shear stress in adverse pressure gradient flow. The $k-\omega$ model by Wilcox and the baseline $k-\omega$ model by Menter lead to acceptable numerical results, while the shear stress transport model by Menter performs poorly.

Chapter 2

The test case

In this chapter we define the test case to be used in the numerical calculations in terms of its geometry and inlet condition. Since previous measurements have been gathered and the test case serves as a benchmark for room air distribution, it is suitable for the purpose of this report. We consider the 2-D isothermal test case described in Nielsen [9]. In the annex 20 room, illustrated in figure 2.1, the air is

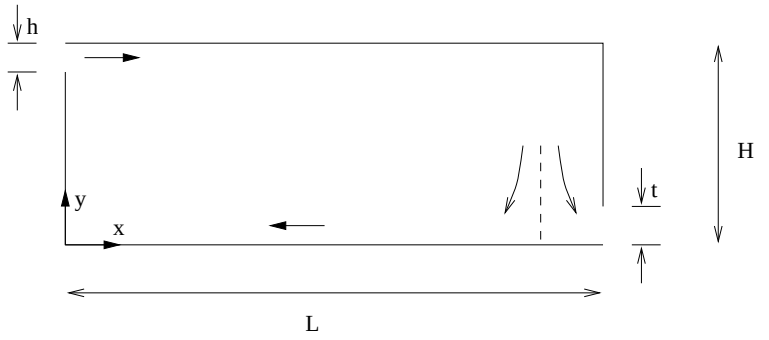

Figure 2.1: The annex 20 2-D isothermal test case.

supplied in the upper left corner and exhausted through the opening to the lower right. The dimensions given in figure 2.1 take the values

$$H = 3.0\ m,\ L = 9.0\ m,\ h = 0.168\ m \text{ and } t = 0.48\ m. \tag{2.1}$$

We use the inlet velocity

$$u_0 = 0.455\ \frac{m}{s}, \tag{2.2}$$

and the kinematic viscosity $\nu = 15.3\ \cdot 10^{-6}\ \frac{m^2}{s}$. This leads to the Reynolds number

$$Re_h = \frac{hu_0}{\nu} = 5000, \tag{2.3}$$

based on the conditions at the supply opening.

According to Nielsen [9], we estimate the turbulent length scale as

$$l_0 = \frac{h}{10} = 0.0168\ m, \tag{2.4}$$

and choose the turbulent intensity $Tu \equiv \frac{\sqrt{\overline{u_i'^2}}}{u_0} = 4\%$. From these values we estimate the inlet condition

$$k_0 = \frac{3}{2}(0.04 \cdot u_0)^2 \approx 4.97\ 10^{-4}\ \frac{m^2}{s^2} \tag{2.5}$$

for the turbulent kinetic energy, and

$$\epsilon_0 = \frac{k_0^{1.5}}{l_0} \approx 6.60\ 10^{-4}\ \frac{m^2}{s^3} \tag{2.6}$$

for the dissipation of turbulent kinetic energy. The inlet condition for the specific dissipation rate ω is specified using the relation

$$\omega_0 = \frac{\epsilon_0}{0.09 k_0} \approx 15\ \frac{1}{s}. \tag{2.7}$$

Equation (2.7) is derived by equating the eddy viscosity for the standard $k-\epsilon$ model to the eddy viscosity for the $k-\omega$ model by Wilcox. In the input file for the flow solver, we specify $Tu = \frac{\sqrt{\overline{u_i'^2}}}{u_0}$ and either l_0 or ω_0, for the $k-\epsilon$ and $k-\omega$ models respectively.

Experimental results for the flow are available along two vertical lines,

$$x = 3.0 \text{ and } x = 6.0, \tag{2.8}$$

and two horizontal lines,

$$y = 0.084 \text{ and } y = 2.916. \tag{2.9}$$

Measurements of the dimensionless horizontal velocity along the four lines mentioned in (2.8) and (2.9) are found in Nielsen [9]. This concludes the presentation of the test case, and we turn to the formulation of the governing equations.

Chapter 3

The governing equations

The governing equation are the continuity and Navier-Stokes equations combined with transport equations for the two quantities turbulent kinetic energy k, and dissipation of turbulent kinetic energy ϵ. In this report the equations are presented using the Einstein summation convention.

3.1 Continuity and Navier-Stokes equations

Assuming that the flow is incompressible, both the continuity equation and the Navier-Stokes equations reduce to

$$\frac{\partial u_i}{\partial x_i} = 0, \tag{3.1}$$

$$\frac{\partial u_i}{\partial t} + u_j \frac{\partial u_i}{\partial x_j} = -\frac{1}{\rho}\frac{\partial p}{\partial x_i} + \nu \frac{\partial^2 u_i}{\partial x_j^2}, \tag{3.2}$$

where x_i, u_i, p, ρ, ν and t, respectively, are position, velocity, pressure, density, kinematic viscosity and time. We decompose the flow quantities, f_i, into

$$f_i(x_i, t) = F_i(x_i) + f_i'(x_i, t_i), \tag{3.3}$$

where $F_i(x,t)$ is the time average and $f_i'(x_i, t_i)$ is the fluctuating part of the quantity. According to Tennekes & Lumley [20], the time average of the quantity, and the time average of the fluctuating part of the quantity is defined respectively by

$$F_i(x) = \lim_{T\to\infty} \frac{1}{T} \int_{t_0}^{t_0+T} f_i(x_i, t_i) dt, \tag{3.4}$$

and

$$\overline{f_i'(x,t)} = \lim_{T\to\infty} \frac{1}{T} \int_{t_0}^{t_0+T} (f_i(x,t) - F_i(x)) dt \equiv 0 \tag{3.5}$$

In this problem f is either the velocity u_i or the pressure p. Introducing (3.3) into (3.1) and time averaging using definition (3.4) and (3.5), we get

$$\overline{\frac{\partial (U_i + u_i')}{\partial x_i}} = \overline{\frac{\partial U_i}{\partial x_i}} + \overline{\frac{\partial u_i'}{\partial x_i}} = \frac{\partial U_i}{\partial x_i} = 0. \tag{3.6}$$

We now insert (3.3) into (3.2), time-averaging and get

$$\overline{\frac{\partial(U_i+u_i')}{\partial t_i}}+\overline{(U_j+u_j')\frac{\partial(U_i+u_i')}{\partial x_j}}=-\overline{\frac{1}{\rho}\frac{\partial(P+p')}{\partial x_i}}+\nu\overline{\frac{\partial^2(U_i+u_i')}{\partial x_j^2}}. \tag{3.7}$$

The second term on the left-hand side leads to the product

$$\overline{u_j'\frac{\partial(u_i')}{\partial x_j}}, \tag{3.8}$$

which, due to continuity, can be rewritten as

$$\frac{\partial\overline{u_i'u_j'}}{\partial x_j}. \tag{3.9}$$

Except from this, all terms involving fluctuating parts of the flow parameters vanish. Therefore, the Reynolds-Averaged Navier-Stokes (RANS) equations can be expressed as

$$\frac{\partial U_i}{\partial t}+U_j\frac{\partial U_i}{\partial x_j}=-\frac{1}{\rho}\frac{\partial P}{\partial x_i}+\frac{\partial}{\partial x_j}\left(\nu\frac{\partial U_i}{\partial x_j}-\overline{u_i'u_j'}\right). \tag{3.10}$$

The term $\overline{u_i'u_j'}$ is a result of the non-linear convective terms, and is referred to as the Reynolds stresses. We need to model this term in order to solve equation (3.10).

The full Reynolds stress tensor is symmetric, and consequently it contains six new unknowns. Deriving transport equations for $\overline{u_i'u_j'}$ from the Navier-Stokes equations gives rise to third order products of the fluctuating velocities. As a consequence, the number of unknowns compared to the number of equations cannot be reduced this way. The latter is known as the closure problem. The problem is circumvented applying the Boussinesq approximation, in which we assume proportionality between the deviatoric part of the Reynolds stress tensor and the strain rate tensor

$$-\overline{u_i'u_j'}=\nu_t\left(\frac{\partial U_i}{\partial x_j}+\frac{\partial U_j}{\partial x_i}\right)-\frac{2}{3}k\delta_{ij}, \tag{3.11}$$

which defines the eddy viscosity ν_t. The assumption is analogous to the constitutive relation presented in Arpaci & Larsen [1]. From dimensional analysis, see e.g. Schmidt [16], the eddy viscosity is modelled as

$$\nu_t=C_\mu f_\mu\frac{k^2}{\epsilon}, \tag{3.12}$$

where C_μ is found empirically to be 0.09 from conditions of equilibrium flow, f_μ is a damping function used to compensate for low Reynolds number effects in near wall regions, k is turbulent kinetic energy, and ϵ is dissipation of turbulent kinetic energy. The divergence of the Reynolds stress tensor (3.11) is

$$-\frac{\partial\overline{u_i'u_j'}}{\partial x_j}=\frac{\partial}{\partial x_j}\left(\nu_t\frac{\partial U_i}{\partial x_j}\right)-\frac{\partial}{\partial x_j}\left(\frac{2}{3}k\delta_{ij}\right), \tag{3.13}$$

which we insert in (3.10), and finally obtain

$$\frac{\partial U_i}{\partial t} + U_j \frac{\partial U_i}{\partial x_j} = -\frac{1}{\rho}\frac{\partial \left(P + \frac{2}{3}\rho k\right)}{\partial x_i} + \frac{\partial}{\partial x_j}\left((\nu + \nu_t)\frac{\partial U_i}{\partial x_j}\right). \tag{3.14}$$

3.2 The k equation

The turbulent kinetic energy k, is defined as $k \equiv \frac{1}{2}\overline{u_i' u_i'}$. A transport equation for k is obtained by multiplying the Navier-Stokes equations with u_i'. Physically, this corresponds to requiring conservation of the mechanical energy connected to the velocity fluctuation. Introducing the decomposed quantities and taking the time-average we obtain

$$\begin{aligned} u_i'\frac{\partial U_i}{\partial t} + u_i'\frac{\partial u_i'}{\partial t} &+ u_i' U_j \frac{\partial U_i}{\partial x_j} + u_i' U_j \frac{\partial u_i'}{\partial x_j} + u_i' u_j' \frac{\partial U_i}{\partial x_j} + u_i' u_j' \frac{\partial u_i'}{\partial x_j} \\ &= -\frac{1}{\rho}\left(u_i'\frac{\partial P}{\partial x_i} + u_i'\frac{\partial p}{\partial x_i}\right) + \nu\left(u_i'\frac{\partial^2 U_i}{\partial x_j^2} + u_i'\frac{\partial^2 u_i'}{\partial x_j^2}\right). \end{aligned} \tag{3.15}$$

Taking the time-average, introducing the transformation

$$\overline{u_i'\frac{\partial u_i'}{\partial x_j}} = \frac{\partial \left(\frac{1}{2}\overline{u_i' u_i'}\right)}{\partial x_j} = \frac{\partial k}{\partial x_j} \tag{3.16}$$

together with continuity, we obtain the transport equation

$$\frac{\partial k}{\partial t} + U_j \frac{\partial k}{\partial x_j} = \underbrace{-\overline{u_i' u_j'}\frac{\partial U_i}{\partial x_j}}_{\mathcal{P}_k} \underbrace{- \frac{\partial}{\partial x_j}\left(\frac{\overline{p' u_j'}}{\rho} + \frac{1}{2}\overline{u_j' u_i' u_i'}\right)}_{\mathcal{D}_k} + \underbrace{\nu \overline{u_i \frac{\partial^2 u_i'}{\partial x_j^2}}}_{\mathcal{V}_k} \tag{3.17}$$

for the turbulent kinetic energy. In (3.17) $\mathcal{P}_k$ is the production of k, $\mathcal{D}_k$ is interpreted as the diffusion of k, and $\mathcal{V}_k$ is the effect of the molecular viscosity.

Applying the Boussinesq approximation (3.11), the production term $\mathcal{P}_k$ is modelled by

$$\begin{aligned} \mathcal{P}_k &= \nu_t\left(\frac{\partial U_i}{\partial x_j} + \frac{\partial U_j}{\partial x_i}\right)\frac{\partial U_i}{\partial x_j} - \frac{2}{3}k\delta_{ij}\frac{\partial U_i}{\partial x_j} \\ &= \nu_t\left(\frac{\partial U_i}{\partial x_j} + \frac{\partial U_j}{\partial x_i}\right)\frac{\partial U_i}{\partial x_j}. \end{aligned} \tag{3.18}$$

The latter reduction occurs due to continuity for the incompressible case. The diffusion term is modelled using a gradient transport hypothesis

$$\mathcal{D}_k = -\frac{\partial}{\partial x_j}\left(\frac{\nu_t}{\sigma_k}\frac{\partial k}{\partial x_j}\right), \tag{3.19}$$

see Speziale *et al* [17]. Here σ_k is the turbulent Prandtl number, normally taken to be unity. Finally, we rewrite the term due to the effect of the molecular viscosity and get

$$\begin{aligned}
\mathcal{V}_k &= \nu\overline{u_i'\frac{\partial^2 u_i'}{\partial x_j^2}} \\
&= \nu\frac{\partial}{\partial x_j}\left(\overline{u_i'\frac{\partial u_i'}{\partial x_j}}\right) - \nu\overline{\frac{\partial u_i'}{\partial x_j}\frac{\partial u_i'}{\partial x_j}} \\
&= \nu\frac{\partial}{\partial x_j}\left(\overline{u_i'\frac{\partial u_i'}{\partial x_j}}\right) - \epsilon,
\end{aligned} \tag{3.20}$$

where ϵ denotes the isotropic dissipation of turbulent kinetic energy.
We insert (3.18), (3.19) and (3.20) in (3.17) and finally obtain

$$\frac{\partial k}{\partial t} + U_j\frac{\partial k}{\partial x_j} = \nu_t\left(\frac{\partial U_i}{\partial x_j} + \frac{\partial U_j}{\partial x_i}\right)\frac{\partial U_i}{\partial x_j} + \frac{\partial}{\partial x_j}\left[\left(\nu + \frac{\nu_t}{\sigma_k}\right)\frac{\partial k}{\partial x_j}\right] - \epsilon. \tag{3.21}$$

3.3 The ϵ equation

In the previous section we defined the dissipation of turbulent kinetic energy as $\epsilon \equiv \nu\overline{\frac{\partial u_i'}{\partial x_j}\frac{\partial u_i'}{\partial x_j}}$. By applying the operator $\nu\frac{\partial u_i'}{\partial x_j}\frac{\partial}{\partial x_j}$ to the Navier-Stokes equations, again introducing the decomposed quantities and taking the time average, we get

$$\begin{aligned}
&\nu\frac{\partial u_i'}{\partial x_j}\frac{\partial}{\partial x_j}\left[\underbrace{\frac{\partial(U_i+u_i')}{\partial t}}_{I} + \underbrace{(U_j+u_j')\frac{\partial(U_i+u_i)}{\partial x_j}}_{II}\right] \\
= \;& \nu\frac{\partial u_i'}{\partial x_j}\frac{\partial}{\partial x_j}\left[\underbrace{\frac{1}{\rho}\frac{\partial(P+p')}{\partial x_i}}_{III} + \underbrace{\nu\frac{\partial^2(U_i+u_i')}{\partial x_j^2}}_{IV}\right].
\end{aligned} \tag{3.22}$$

From (3.22) we now derive the ϵ-equation. To maintain the overview we follow the rigorous procedure used by Schmidt in [16]. We write the terms in their full extent

and obtain

$$I: \quad \nu\overline{\frac{\partial u_i'}{\partial x_j}\frac{\partial^2 U_i}{\partial x_j \partial t}} + \overline{\frac{\partial u_i'}{\partial x_j}\frac{\partial^2 u_i'}{\partial x_j \partial t}} = 0 + \frac{1}{2}\frac{\partial \epsilon}{\partial t} \tag{3.23}$$

$$\begin{aligned} II: \quad & \nu\overline{\frac{\partial u_i'}{\partial x_k}\frac{\partial}{\partial x_k}\left(U_j\frac{\partial U_i}{\partial x_j}\right)} + \nu\overline{\frac{\partial u_i'}{\partial x_k}\frac{\partial}{\partial x_k}\left(U_j\frac{\partial u_i'}{\partial x_j}\right)} \\ + \; & \nu\overline{\frac{\partial u_i'}{\partial x_k}\frac{\partial}{\partial x_k}\left(u_j'\frac{\partial U_i}{\partial x_j}\right)} + \nu\overline{\frac{\partial u_i'}{\partial x_k}\frac{\partial}{\partial x_k}\left(u_j'\frac{\partial U_i}{\partial x_j}\right)} \\ = \; & 0 + \nu\frac{\partial U_j}{\partial x_k}\overline{\frac{\partial u_i'}{\partial x_j}\frac{\partial u_i'}{\partial x_k}} + \nu U_j\overline{\frac{\partial}{\partial x_j}\left[\frac{1}{2}\left(\frac{\partial u_i'}{\partial x_k}\right)^2\right]} \\ + \; & \nu\frac{\partial U_i}{\partial x_j}\overline{\frac{\partial u_i'}{\partial x_k}\frac{\partial u_j'}{\partial x_k}} + \nu\frac{\partial^2 U_j}{\partial x_j \partial x_k}\overline{u_j'\frac{\partial u_i'}{\partial x_k}} \\ + \; & \nu\overline{\frac{\partial u_i'}{\partial x_j}\frac{\partial u_i'}{\partial x_k}\frac{\partial u_j'}{\partial x_k}} + \nu\overline{u_j'\frac{\partial}{\partial x_j}\left[\frac{1}{2}\left(\frac{\partial u_i'}{\partial x_k}\right)^2\right]} \\ = \; & \frac{1}{2}U_j\frac{\partial \epsilon}{\partial x_j} + \nu\frac{\partial U_i}{\partial x_k}\left(\frac{\partial u_i'}{\partial x_j}\frac{\partial u_i'}{\partial x_k} + \frac{\partial u_i'}{\partial x_j}\frac{\partial u_k'}{\partial x_j}\right) + \nu\frac{\partial^2 U_j}{\partial x_j \partial x_k}\overline{u_j'\frac{\partial u_i'}{\partial x_k}} \\ + \; & \nu\overline{\frac{\partial}{\partial x_j}\left[u_j'\frac{1}{2}\left(\frac{\partial u_i'}{\partial x_k}\right)^2\right]} + \nu\overline{\frac{\partial u_i'}{\partial x_j}\frac{\partial u_i'}{\partial x_k}\frac{\partial u_j'}{\partial x_k}} \end{aligned} \tag{3.24}$$

$$III: \quad -\frac{\nu}{\rho}\left[\overline{\frac{\partial u_i'}{\partial x_j}\frac{\partial^2 P}{\partial x_i \partial x_j}} + \overline{\frac{\partial u_i'}{\partial x_j}\frac{\partial^2 p'}{\partial x_i \partial x_j}}\right] = -\frac{\nu}{\rho}\overline{\frac{\partial}{\partial x_i}\left(\frac{\partial u_i'}{\partial x_j}\frac{\partial p'}{\partial x_j}\right)} \tag{3.25}$$

$$\begin{aligned} IV: \quad & \nu^2\overline{\frac{\partial u_i'}{\partial x_k}\frac{\partial^3 U_i}{\partial x_j \partial x_j \partial x_k}} + \nu^2\overline{\frac{\partial u_i'}{\partial x_k}\frac{\partial^3 u_i'}{\partial x_j \partial x_j \partial x_k}} \\ = \; & 0 + \nu^2\overline{\frac{\partial u_i'}{\partial x_k}\frac{\partial^3 u_i}{\partial x_j \partial x_j \partial x_k}} \\ = \; & \nu^2\frac{\partial^2}{\partial x_j \partial x_j}\left[\frac{1}{2}\overline{\left(\frac{\partial u_i'}{\partial x_k}\right)^2}\right] - \nu^2\overline{\left(\frac{\partial^2 u_i'}{\partial x_j \partial x_k}\right)^2} \\ = \; & \frac{\nu}{2}\frac{\partial^2 \epsilon}{\partial x_j^2} - \nu^2\overline{\left(\frac{\partial^2 u_i'}{\partial x_j \partial x_k}\right)^2}. \end{aligned} \tag{3.26}$$

We introduce (3.23)-(3.26) into (3.22) and obtain

$$\frac{D\epsilon}{Dt} = \mathcal{P}_\epsilon - \Phi_\epsilon - \mathcal{D}_\epsilon + \mathcal{D}_v, \tag{3.27}$$

where

$$\begin{aligned}
\frac{D\epsilon}{Dt} &= \frac{\partial \epsilon}{\partial t} + U_j \frac{\partial \epsilon}{\partial x_j}, \\
\mathcal{P}_\epsilon &= -2\nu \frac{\partial U_i}{\partial x_k} \left(\frac{\partial u_i'}{\partial x_j} \frac{\partial u_i'}{\partial x_k} + \frac{\partial u_i'}{\partial x_j} \frac{\partial u_k'}{\partial x_j} \right) \\
&- 2\nu \overline{\frac{\partial u_i'}{\partial x_j} \frac{\partial u_i'}{\partial x_k} \frac{\partial u_j'}{\partial x_k}} - 2\nu \frac{\partial^2 U_j}{\partial x_j \partial x_k} \overline{u_j' \frac{\partial u_i'}{\partial x_k}}, \\
\Phi_\epsilon &= \nu^2 \overline{\left(\frac{\partial^2 u_i'}{\partial x_j \partial x_k} \right)^2}, \\
\mathcal{D}_\epsilon &= -\frac{2\nu}{\rho} \overline{\frac{\partial}{\partial x_i} \left(\frac{\partial u_i \prime}{\partial x_j} \frac{\partial p'}{\partial x_j} \right)} + \nu \overline{\frac{\partial}{\partial x_j} \left[u_j' \left(\frac{\partial u_i'}{\partial x_k} \right)^2 \right]}, \\
\mathcal{D}_v &= \nu \frac{\partial^2 \epsilon}{\partial x_j^2}.
\end{aligned}$$

The four terms on the right-hand side of (3.27) are respectively production, dissipation, turbulent diffusion and viscous diffusion of the dissipation of turbulent kinetic energy. Due to the complexity of the terms in (3.27), the production and dissipation are modelled by multiplying the corresponding terms in the transport equation for k with $\frac{\epsilon}{k}$, a constant and a damping function. The damping function is introduced to ensure correct behaviour of ϵ near the walls. The turbulent diffusion is modelled using a gradient transport hypothesis similar to that of the k equation. Hence the transport equation (3.27) now becomes

$$\frac{D\epsilon}{Dt} = C_{\epsilon 1} f_1 \frac{\epsilon}{k} \left(-\overline{u_i' u_j'} \right) \frac{\partial U_i}{\partial x_j} + \frac{\partial}{\partial x_j} \left[\left(\nu + \frac{\nu_t}{\sigma_\epsilon} \right) \frac{\partial \epsilon}{\partial x_j} \right] - C_{\epsilon 2} f_2 \frac{\epsilon^2}{k}, \tag{3.28}$$

where σ_ϵ is the turbulent Prandtl number.

Chapter 4

Two-equation turbulence models

In the literature, numerous refinements for the turbulence models have been suggested. It is not in the scope of this text to discuss all these, though some are of interest. Since we consider an internal flow, attention will be paid to near-wall behaviour of turbulent flows, damping functions and the boundary conditions. Furthermore, we describe variables and constants occurring in the turbulence models chosen for testing. We distinguish between two types of turbulence model, low and high Reynolds number models. In the former the transport equations for the model variables are integrated to the walls, while for the latter we use the log-law to approximate turbulent quantities close to the walls.

4.1 Adjustment of the turbulence models

4.1.1 Near-wall behaviour

To carry out near-wall asymptotic analysis for the different terms in the transport equations, we introduce the Taylor series expansion for the fluctuating velocity components

$$u' = a_1 y + a_2 y^2 + \ldots, \tag{4.1}$$
$$v' = b_2 y^2 + b_3 y^3 \ldots, \tag{4.2}$$
$$w' = c_1 y + c_2 y^2 + \ldots, \tag{4.3}$$

where y is the direction normal to the wall. Due to no-slip $a_0 = b_0 = c_0 = 0$, and from continuity $b_1 = 0$. From (4.1)-(4.3) it is a straightforward matter to show that

$$k = \mathcal{O}(y^2), \quad \epsilon = \mathcal{O}(1). \tag{4.4}$$

The near-wall behaviour of a number of other terms is found in Speziale *et al* [17]. It is obvious that reliable numerical results for near-wall flows are only to be expected from turbulence models containing asymptotic consistency with (4.4).

4.1.2 Damping functions

Improved prediction of the flow close to solid boundaries can be obtained using damping functions to adjust the model equations. The function f_μ is introduced to dampen the eddy viscosity in regions near the walls. Applying asymptotic analysis presented in the previous section, it is easily found from (4.4), that $f_\mu = \mathcal{O}\left(\frac{1}{y}\right)$. Furthermore we require that f_μ approaches one as we increase the distance from the wall. The expression for f_μ is obtained using experiments or direct numerical simulation. The same considerations can be applied for the damping functions f_1 and f_2 appearing in (3.28), see e.g. Speziale *et al* [17].

4.1.3 Boundary conditions

Another important numerical problem that occurs is the absence of natural boundary conditions for the dissipation of turbulent kinetic energy. Various proposals for boundary conditions that circumvent this problem have been suggested over the years. The boundary conditions mentioned below are described in details in Speziale *et al* [17].

As a rigorous consequence of the transport equation for the turbulent kinetic energy, we could use the boundary condition

$$\nu \frac{\partial^2 k}{\partial y^2} = \epsilon. \tag{4.5}$$

Since (4.5) contains second order derivatives of k, this leads to considerable numerical stiffness. An alternative version of (4.5) is

$$2\nu \left(\frac{\partial \sqrt{k}}{\partial y} \right) = \epsilon. \tag{4.6}$$

Even though the numerical properties are improved, they are still not satisfactory. Alternatively, the Neumann boundary condition

$$\frac{\partial \epsilon}{\partial y} = 0, \tag{4.7}$$

with improved numerical robustness is commonly used. However, this is completely ad hoc and cannot be justified, neither theoretically nor experimentally.

As a final remark we mention that the balance of terms at the walls involves higher order correlation which exacerbates the problem with numerical stiffness. This problem is discussed in further details in Speziale *et al* [17].

The above describes some of the problems that have to be taken into account when using turbulence models in the simulations. The list is by no means complete, but contains the topics that are most relevant for the flow considered in this report. We now present the different models chosen for testing. For additional information concerning the models, see e.g. Schmidt [16].

4.2 Standard $k-\epsilon$ model

For this model the transport equations for the turbulent quantities take the form

$$\frac{Dk}{Dt} = \frac{\tau_{ij}}{\rho}\frac{\partial U_i}{\partial x_j} + \frac{\partial}{\partial x_j}\left[(\nu + \frac{\nu_t}{\sigma_k})\frac{\partial k}{\partial x_j}\right] - \epsilon \tag{4.8}$$

$$\frac{D\epsilon}{Dt} = C_{\epsilon 1}\frac{\epsilon}{k}\frac{\tau_{ij}}{\rho}\frac{\partial U_i}{\partial x_j} + \frac{\partial}{\partial x_j}\left[(\nu + \frac{\nu_t}{\sigma_\epsilon})\frac{\partial \epsilon}{\partial x_j}\right] - C_{\epsilon 2} f_2 \frac{\epsilon^2}{k}. \tag{4.9}$$

The eddy viscosity is

$$\nu_t = C_\mu f_\mu \frac{k^2}{\epsilon}. \tag{4.10}$$

The model constants are

$$\begin{aligned} C_\mu = 0.09 \quad \sigma_k = 1.0 \quad \sigma_\epsilon = 1.3 \\ C_{\epsilon 1} = 1.44 \quad C_{\epsilon 2} = 1.92, \end{aligned} \tag{4.11}$$

and the damping functions

$$f_\mu = f_2 = 1. \tag{4.12}$$

In the model the transport equations are not integrated to the walls. Instead the production and dissipation of kinetic energy are specified in the near-wall cell, using the logarithmic law-of-the-wall. The value of ϵ is specified the same way. A more detailed description of the wall laws can be found in Sørensen [18].

4.3 Low Reynolds number $k-\epsilon$ model by Launder & Sharma

A low-Reynolds number $k-\epsilon$ model is presented by Launder & Sharma in [3]. A new variable $\tilde{\epsilon}$ is defined as

$$\epsilon = \tilde{\epsilon} + D \qquad D = 2\nu\left(\frac{\partial\sqrt{k}}{\partial n}\right)^2, \tag{4.13}$$

where n is the direction normal to the wall. Compared to ϵ, $\tilde{\epsilon}$ has the advantage of the natural boundary condition $\tilde{\epsilon} = 0$, at the walls. For addition, it is proposed by Launder & Sharma that the term

$$E = 2\nu\nu_t\left(\frac{\partial^2 U}{\partial y^2}\right)^2, \tag{4.14}$$

is added to the right-hand side of the transport equation for ϵ. The term is added to compensate for additional production and to further balance diffusion and dissipation in the vicinity of the walls. With the new variable (4.13) and the term (4.14),

the transport equations for the turbulent variables becomes

$$\frac{Dk}{Dt} = \frac{\tau_{ij}}{\rho}\frac{\partial U_i}{\partial x_j} + \frac{\partial}{\partial x_j}\left[(\nu + \frac{\nu_t}{\sigma_k})\frac{\partial k}{\partial x_j}\right] - (\tilde{\epsilon} + D) \tag{4.15}$$

$$\frac{D\tilde{\epsilon}}{Dt} = C_{\epsilon 1}\frac{\tilde{\epsilon}}{k}\frac{\tau_{ij}}{\rho}\frac{\partial U_i}{\partial x_j} + \frac{\partial}{\partial x_j}\left[(\nu + \frac{\nu_t}{\sigma_{\tilde{\epsilon}}})\frac{\partial \tilde{\epsilon}}{\partial x_j}\right] - C_{\epsilon 2} f_2 \frac{\tilde{\epsilon}^2}{k} + E. \tag{4.16}$$

The eddy viscosity is defined as

$$\nu_t = C_\mu f_\mu \frac{k^2}{\tilde{\epsilon}}. \tag{4.17}$$

The term D is approximated as follows

$$D = 2\nu\left(\frac{\partial\sqrt{k}}{\partial n}\right)^2 \approx 2\nu\left(\nabla\sqrt{k}\right)^2. \tag{4.18}$$

The constants are

$$\begin{aligned} C_\mu = 0.09 \quad \sigma_k = 1.0 \quad \sigma_\epsilon = 1.3 \\ C_{\epsilon 1} = 1.44 \quad C_{\epsilon 2} = 1.92, \end{aligned} \tag{4.19}$$

and the damping functions are both functions of the turbulent Reynolds number

$$R_t = \frac{k^2}{\nu\tilde{\epsilon}}. \tag{4.20}$$

The damping function for the eddy viscosity is

$$f_\mu = \exp\left[\frac{-3.4}{(1 + \frac{R_t}{50})^2}\right], \tag{4.21}$$

and the damping function for the dissipation term in (4.16) is

$$f_2 = 1 - 0.3\exp(-R_t^2). \tag{4.22}$$

The boundary conditions at the walls are

$$k_w = 0 \quad \text{and} \quad \tilde{\epsilon}_w = 0. \tag{4.23}$$

4.4 $k - \omega$ model by Wilcox

Already in 1942 Kolmogoroff suggested the specific dissipation rate ω with dimension $time^{-1}$ as an alternative to ϵ. In 1988 Wilcox [21] presented his $k - \omega$ model based on the original transport equation by Kolmogoroff. The noteworthy property of this

model is that the demand for damping functions in near-wall regions is rendered superfluous. The transport equations are

$$\frac{Dk}{Dt} = \frac{\tau_{ij}}{\rho}\frac{\partial U_i}{\partial x_j} + \frac{\partial}{\partial x_j}\left[(\nu + \sigma_{k1}\nu_t)\frac{\partial k}{\partial x_j}\right] - \beta^*\omega k \tag{4.24}$$

$$\frac{D\omega}{Dt} = \frac{\gamma_1}{\rho\nu_t}\tau_{ij}\frac{\partial U_i}{\partial x_j} + \frac{\partial}{\partial x_j}\left[(\nu + \sigma_{\omega 1}\nu_t)\frac{\partial \omega}{\partial x_j}\right] - \beta_1\omega^2. \tag{4.25}$$

The eddy viscosity is defined as

$$\nu_t = \frac{k}{\omega}, \tag{4.26}$$

and the model constants are

$$\sigma_{k1} = 0.5 \quad \sigma_{\omega 1} = 0.5 \quad \beta_1 = 0.0750 \quad \beta^* = 0.09$$
$$\kappa = 0.41 \quad \gamma_1 = \frac{\beta_1}{\beta^*} - \sigma_{\omega 1}\frac{\kappa^2}{\sqrt{\beta^*}}. \tag{4.27}$$

The boundary conditions are

$$k_w = 0 \quad \text{and} \quad \omega_w = 10\frac{6\nu}{\beta_1(\Delta y)^2}, \tag{4.28}$$

where Δy is the distance to the nearest point from the wall. In the first grid point above surface we require $y^+ < 3$, for (4.28) to be applicable. The boundary conditions are suggested by Menter [5], who also proposed that a limiter is applied to the production term in the k equation. This should relieve excessive production of turbulent kinetic energy and numerical 'wiggles'. The limiter takes the form.

$$\tilde{\mathcal{P}}_k = min(\mathcal{P}; 20\mathcal{D}_k), \tag{4.29}$$

where $\mathcal{D}_k$ is dissipation of turbulent kinetic energy.

4.5 $k-\omega$ BSL model by Menter

The $k-\omega$ model by Wilcox has the disadvantage of being highly sensitive to ω specified in the freestream, see Menter [6]. For the same reason Menter [6] proposed the $k-\omega$ baseline (BSL) model, combining the $k-\omega$ model by Wilcox in the inner region of the boundary layer, and the standard $k-\epsilon$ in the outer region and the free stream. The transport equations for the baseline model by Menter are

$$\frac{Dk}{Dt} = \frac{\tau_{ij}}{\rho}\frac{\partial U_i}{\partial x_j} + \frac{\partial}{\partial x_j}\left[(\nu + \sigma_k\nu_t)\frac{\partial k}{\partial x_j}\right] - \beta^*\omega k \tag{4.30}$$

$$\frac{D\omega}{Dt} = \frac{\gamma}{\rho\nu_t}\tau_{ij}\frac{\partial U_i}{\partial x_j} + \frac{\partial}{\partial x_j}\left[(\nu + \sigma_\omega\nu_t)\frac{\partial \omega}{\partial x_j}\right] + 2(1-F_1)\sigma_{\omega 2}\frac{1}{\omega}\frac{\partial k}{\partial x_j}\frac{\partial \omega}{\partial x_j}. \tag{4.31}$$

The transport equations are obtained by transforming the $k-\epsilon$ model into a $k-\omega$ formulation, and using the blending function F_1. The blending function is designed

to be one near walls and zero away from surfaces. Compared to the transport equation (4.25), equation (4.31) differs by the appearance of an additional cross-diffusion term. We use the eddy viscosity

$$\nu_t = \frac{k}{\omega}. \tag{4.32}$$

The inner constants are

$$\begin{aligned} \sigma_{k1} = 0.5 \quad \sigma_{\omega 1} = 0.5 \quad \beta_1 = 0.0750 \quad \beta^* = 0.09 \\ \kappa = 0.41 \quad \gamma_1 = \frac{\beta_1}{\beta^*} - \sigma_{\omega 1}\frac{\kappa^2}{\sqrt{\beta^*}}, \end{aligned} \tag{4.33}$$

which are similar to those of the $k-\omega$ model by Wilcox. The outer constants are

$$\begin{aligned} \sigma_{k2} = 1.0 \quad \sigma_{\omega 2} = 0.856 \quad \beta_2 = 0.0828 \quad \beta^* = 0.09 \\ \kappa = 0.41 \quad \gamma_2 = \frac{\beta_2}{\beta^*} - \sigma_{\omega 2}\frac{\kappa^2}{\sqrt{\beta^*}}, \end{aligned} \tag{4.34}$$

corresponding to the standard $k-\epsilon$ model. The constants for the inner model ϕ_1, and the outer model ϕ_2, are mixed to give ϕ using the blending function F_1. We get

$$\phi = F_1\phi_1 + (1 - F_1)\phi_2, \tag{4.35}$$

where

$$F_1 = \tanh(\arg_1^4). \tag{4.36}$$

Here

$$\arg_1 = min\left[max\left(\frac{\sqrt{k}}{0.09\omega y}; \frac{500\nu}{y^2\omega}\right); \frac{4\sigma_{\omega 2}k}{CD_{k\omega}y^2}\right], \tag{4.37}$$

where y is the distance to the wall and

$$CD_{k\omega} = max\left(2\sigma_{\omega 2}\frac{1}{\omega}\frac{\partial k}{\partial x_j}\frac{\partial \omega}{\partial x_j}, 10^{-20}\right). \tag{4.38}$$

The boundary conditions are

$$k_w = 0 \quad \text{and} \quad \omega_w = 10\frac{6\nu}{\beta_1(\Delta y)^2}, \tag{4.39}$$

identical to (4.28).

4.6 $k-\omega$ SST model by Menter

The Shear Stress Transport (SST) model is identical to the baseline model, except that the constants for the inner model are changed to

$$\begin{aligned} \sigma_{k1} = 0.85 \quad \sigma_{\omega 1} = 0.5 \quad \beta_1 = 0.0750 \quad \beta^* = 0.09 \\ \kappa = 0.41 \quad \gamma_1 = \frac{\beta_1}{\beta^*} - \sigma_{\omega 1}\frac{\kappa^2}{\sqrt{\beta^*}}, \quad a_1 = 0.31, \end{aligned} \tag{4.40}$$

and the eddy viscosity is now defined as

$$\nu_t = \frac{a_1 k}{max(a_1\omega; \Omega F_2)}, \tag{4.41}$$

where

$$F_2 = \tanh(\arg_2^2) \tag{4.42}$$

and

$$\arg_2 = max\left(2\frac{\sqrt{k}}{0.09\omega y}; \frac{500\nu}{y^2\omega}\right). \tag{4.43}$$

The modified eddy viscosity accounts for the transport of principal turbulent shear stress, τ. According to Menter [6], the new eddy viscosity leads to improvement in performance compared to the $k-\omega$ model by Wilcox, as well as the standard $k-\epsilon$ model.

Chapter 5

Solution procedure

The numerical code is a 2-D finite volume code in general curvilinear coordinates, based on the Basis2D platform developed by Michelsen [7] and Sørensen [18]. We solve the Reynolds averaged isothermal incompressible Navier-Stokes equations using block structured, cell centered and non-staggered grids. The convective terms are discretized using a second order upwind difference scheme (SUDS). For the $k-\epsilon$ models we use SUDS without limiter, while a limiter is added to the $k-\omega$ models, in order to avoid 'wiggles' at the expense of increased numerical diffusion.

In the solution procedure we first have the predictor step, in which the linearized decoupled equations for the variables U_i and P are solved. In the following corrector step, continuity is enforced by adjusting pressure to get the right mass flux through the cell-faces. The procedure is known as the SIMPLE algorithm, described by Patankar & Spalding in [13]. The transport equations are solved using a TDMA solver in alternating direction. The pressure correction equation can be solved quicker using a multigrid technique. The overall calculation time is further reduced applying a three level grid sequence. Using under-relaxation, convergence properties are improved, and pressure decoupling is avoided applying the Rhie/Chow interpolation technique, see Rhie [14].

Chapter 6

Computational grid

6.1 Hyperbolic netstretch

In this section a function for hyperbolic netstretch is suggested, based on a hyperbolic tangent function. Denoting the start and ending points for the mesh by y_0 and y_1, respectively, a general function for the distribution of the points may be written as

$$y = y_0 + (y_1 - y_0)f, \tag{6.1}$$

where the function f lies in the interval from zero to one, both included. Using hyperbolic tangent functions, three variations of the function f may be used, depending on the desire to stretch towards both zero and one, towards zero only or towards one only. Using the information that $f(j = 1) = 0$ and $f(j = ny) = 1$, the three functions can be described as

$$f(j) = \frac{tanh\left(K\left(\frac{2(j-1)}{ny-1} + K_1\right)\right) - tanh\left(K \cdot K_1\right)}{tanh\left(K\left(2 + K_1\right)\right) - tanh\left(K \cdot K_1\right)}, \tag{6.2}$$

$$f(j) = \frac{tanh\left(K\left(\frac{j-1-(ny-1)}{ny-1}\right)\right)}{tanh(K)} + 1, \tag{6.3}$$

and

$$f(j) = \frac{tanh\left(K\left(\frac{j-1}{ny-1}\right)\right)}{tanh(K)}, \tag{6.4}$$

respectively. K and K_1 in (6.2) is determined by the required cell heights in the first and last cell, K in (6.3) by the required cell height in the first cell and K in (6.4) by the cell height in the last cell.

Using the function stretching towards both ends, (6.2), as an example, and denoting the required cell heights in the first and last cell by s_0 and s_1, respectively, (6.2) for the first and last cell becomes

$$f(2) = \frac{tanh\left(K\left(\frac{2}{ny-1} + K_1\right)\right) - tanh\left(K \cdot K_1\right)}{tanh\left(K\left(2 + K_1\right)\right) - tanh\left(K \cdot K_1\right)} = S_0, \tag{6.5}$$

and

$$f(ny-1) = \frac{tanh\left(K\left(\frac{2(ny-2)}{ny-1} + K_1\right)\right) - tanh\left(K \cdot K_1\right)}{tanh\left(K\left(2 + K_1\right)\right) - tanh\left(K \cdot K_1\right)} = 1 - S_1, \tag{6.6}$$

where S_0 and S_1 are the original values of s_0 and s_1 divided by $(y_1 - y_0)$. For use with the Newton-Raphson method, the equations may be rewritten as

$$F(1) = S_0 - \frac{tanh\left(K\left(\frac{2}{ny-1} + K_1\right)\right) - tanh\left(K \cdot K_1\right)}{tanh\left(K\left(2 + K_1\right)\right) - tanh\left(K \cdot K_1\right)}, \tag{6.7}$$

and

$$F(2) = 1 - S_1 - \frac{tanh\left(K\left(\frac{2(ny-2)}{ny-1} + K_1\right)\right) - tanh\left(K \cdot K_1\right)}{tanh\left(K\left(2 + K_1\right)\right) - tanh\left(K \cdot K_1\right)}. \tag{6.8}$$

Thus, by solving the non-linear system of equations governed by (6.7) and (6.8), the coefficients K and K_1 can be found. The solution is performed by standard methods. After determination of K and K_1, the equations (6.1) and (6.2) are used to calculate the grid-point positions. Similar procedures are carried out for the functions stretching towards one end only. Here only one unknown K value exist.

6.2 Dimensionless sublayer-scaled distance

The dimensionless sublayer-scaled distance y^+, is the most common parameter for evalution of netstretch towards walls. The definition is

$$y^+ = \frac{u_\tau \Delta y}{\nu}, \tag{6.9}$$

where Δy is the normal distance from the wall to the first grid point, ν is the kinematic viscosity and u_τ is the friction velocity

$$u_\tau = \sqrt{\frac{\tau_w}{\rho}}, \tag{6.10}$$

in which ρ is the density of the fluid and the wall shear stress is defined as

$$\tau_w = \nu\rho\frac{du}{dy}. \tag{6.11}$$

Assuming that the velocity varies linearly from zero to the first grid point, we get

$$\tau_w = \nu\rho\frac{u_1}{\Delta y}, \tag{6.12}$$

in which Δy is the distance to the first grid point above the surface and u_1 is the computed velocity in this point. Using a low-Reynolds number turbulence model, (6.12) apply, and y^+ is easily determined from (6.9). For a high-Reynolds number model the wall shear stress can not be estimated using (6.11). Instead introducing the dimensionless velocity

$$u^+ = \frac{u}{u_\tau}, \tag{6.13}$$

and the law of the wall for an incompressible boundary layer

$$u^+ \approx \frac{1}{\kappa}\ln(y^+) + B, \tag{6.14}$$

see Wilcox [22]. We use $\kappa \approx 0.41$ and $B \approx 5.0$ for the *Karman constant* and the dimensionless constant, respectively. Introducing (6.9) and (6.13) into (6.14) yields

$$\frac{u_1\Delta y}{y^+\nu} = \frac{1}{\kappa}\ln y^+ + B, \tag{6.15}$$

considering now the first grid point above the surface. The non-linear equation (6.15) is solved by standard methods.

For low-Reynolds number turbulence models y^+ should be kept below 1, and for the high-Reynolds number models we require $30 < y^+ < 100$.

6.3 The computational domain

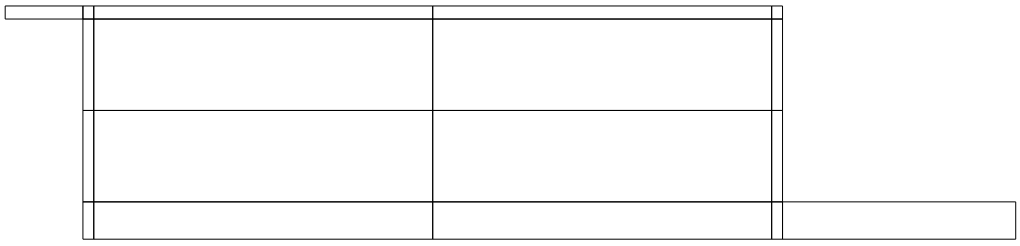

Figure 6.1: The boundaries and blocks for the computational domain.

Here a brief discussion of the computational domain, see figure 6.1, is given. For numerical reasons a short inlet and outlet is added to the geometry of the testcase shown in figure 2.1. With no inlet, an abrupt change in velocity occurs in the supply opening. This is smoothened adding an inlet of length $L_{inlet} = \frac{L}{9}$. A small

recirculation zone occurs in the first part of the outlet. Since *Ellipsys2D* uses the Neumann boundary condition at the outlet, numerical problems occur if air is supplied through an outlet boundary. The problem is circumvented designing an outlet containing the entire recirculation zone, here we choose $L_{outlet} = \frac{L}{3}$

The grid for *EllipSys2D* is build from 18 blocks all containing j^2 grid points. To ensure a satisfying resolution of both the boundary layer along solid boundaries and the shear layer caused by the inlet, the blocks are arranged as shown in figure 6.1. Hyperbolic netstretch in one or two directions is used in all blocks. When stretching, y_0 and y_1 are fixed due to the block boundaries, while s_0 and s_1 are chosen to give $y^+ < 1$ along solid boundaries for the low Reynolds number models and $y^+ > 11$ for the high Reynolds number models. Stretching towards the inner block boundaries ensures that the distance to the first grid point is the same on each side of the boundary. It is our experience that the distance to the first grid point along the solid boundaries should be

$$\Delta y_{left} \approx 0.0007, \quad \Delta y_{floor} \approx 0.0006, \quad \Delta y_{right} \approx 0.0007, \quad \Delta y_{ceiling} \approx 0.0002, \quad (6.16)$$

for $y^+ < 1$ to apply everywhere. Similarly we experienced that the the requirement $y^+ > 11$ is fulfilled almost everywhere, if

$$\Delta y_{left} \approx 0.01, \quad \Delta y_{floor} \approx 0.0016, \quad \Delta y_{right} \approx 0.01, \quad \Delta y_{ceiling} \approx 0.0016. \quad (6.17)$$

For the given arrangement of the blocks, it was not possible to design a grid with both a satisfying resolution of the wall jet and $30 < y^+ < 100$.

Finding a grid independent solution the number of points j are increased until the change in horizontal velocity profiles along the four lines given in (2.8) and (2.9) can be neglected for increased j. This is evaluated by inspection.

In appendix A the number of points required to obtain a grid independent solution is determined for the various models. The result is summarized in table 6.1. It was not possible to obtain a grid independent solution for the $k-\omega$ SST model by Menter. In the next chapter we use the results obtained with the 32x32 grid for this model

In figure 6.2 an example of a grid is given.

Turbulence model	j	Total number of grid points
Standard $k-\epsilon$ model	16	4608
$k-\epsilon$ model by Launder & Sharma	32	18432
$k-\omega$ model by Wilcox	32	18432
$k-\omega$ BSL model by Menter	32	18432
$k-\omega$ SST model by Menter	–	–

Table 6.1: Number of grid points required to obtain a grid independent solution for the considered turbulence models.

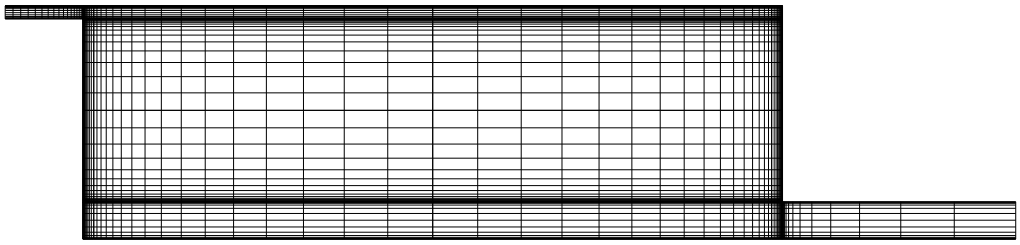

Figure 6.2: Computational grid consisting of 18 blocks each with 16^2 grid points.

Chapter 7

Results

We now present the numerical results obtained, using the five different turbulence models for the testcase presented in chapter 2. For the two-equation turbulence models introduced in chapter 4, we use the following abbreviations

$k-\epsilon$ HI RE	:	Standard $k-\epsilon$ model
$k-\epsilon$ LS	:	$k-\epsilon$ low Reynolds number model by Launder & Sharma
$k-\omega$ ORG	:	$k-\omega$ model by Wilcox
$k-\omega$ BSL	:	$k-\omega$ BSL model by Menter
$k-\omega$ SST	:	$k-\omega$ SST model by Menter.

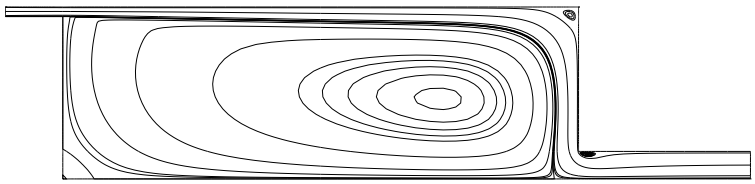

Figure 7.1: Typical picture of streamlines using the models $k-\epsilon$ HI RE, $k-\epsilon$ LS, $k-\omega$ ORG or $k-\omega$ BSL.

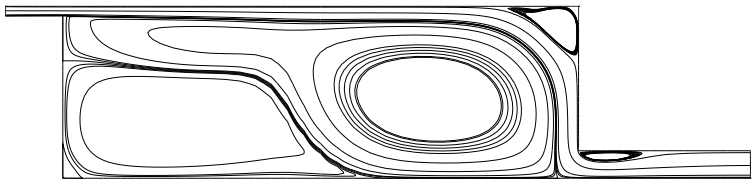

Figure 7.2: Typical picture of streamlines using $k-\omega$ SST model.

7.1 Comparing velocities

In figure 7.3 and 7.4 computed velocities at the positions $x = 3.0$ and $x = 6.0$ are compared with measurements. At $x = 3.0$, figure 7.3(a) and figure 7.4(a), the low Reynolds number models tend to overpredict the velocity close to the ceiling, while the standard $k - \epsilon$ model is in good agreement. Near $y = 2.5$ all the models slightly underpredict the velocity, worst for the $k - \omega$ SST. Close to the floor the two $k - \epsilon$ models show good accordance with measurements, while the $k - \omega$ ORG and the $k - \omega$ BSL underpredict the velocity and the velocity computed with the $k - \omega$ SST has the wrong sign.
At the position $x = 6.0$, figure 7.3(b) and figure 7.4(b), the standard $k - \epsilon$ model underpredicts the velocity close to ceiling. The low Reynolds number models show good agreement here. At $y = 2.5$ all the models show better accordance with measurements than for $x = 3$. Though a relative strong discrepancy has now occured close to $y = 1$. Since the same deviation is predicted by all the models, we have reason to believe that the phenomenon is a three dimensional effect. So could be the case for $x = 3$ and $y = 2.5$. Except from the $k - \omega$ SST all the models fit the measurements well close to the floor.

In figures 7.5 and 7.6 computed velocities are compared with measurements at the positions $y = 0.084$ close to the floor, and $y = 2.916$ close to the ceiling. Close to the ceiling, figure 7.5(b) and 7.6(b), the best agreement between measurements and computation is found for the low Reynolds number models. However, a clear discrepancy between measurements and computations is found close to the boundary of the recirculation zone in the upper right corner of the room. The phenomenon is common for all the models, but it seems as if the passage from the main flow to the small recirculation zone is predicted best by the $k - \epsilon$ LS. Close to the floor, figure 7.5(a) and figure 7.6(a), the standard $k - \epsilon$ model shows better agreement with masurements than the low Reynolds number models. The $k - \omega$ SST shows very poor accordance with measurements close to the floor. From figure 7.6(a), we observe that the $k - \omega$ ORG and the $k - \omega$ BSL predict a steep drop in the velocity at $x \approx 2.5$. This phenomenon is observed neither in the $k - \epsilon$ models nor in the measurements.

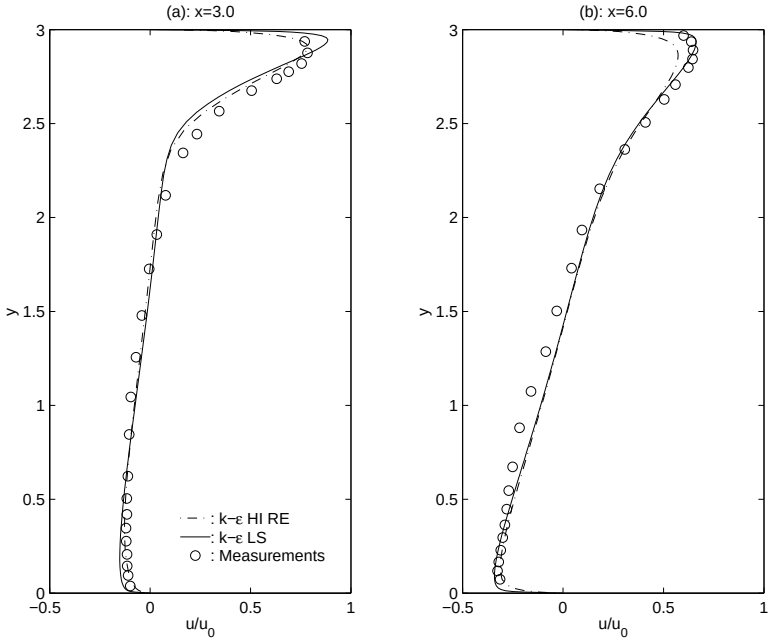

Figure 7.3: Dimensionless velocities $\frac{u}{u_0}$ along two vertical lines for the $k-\epsilon$ HI RE and $k-\epsilon$ LS. Measurements along the same lines in the symmetry plane of the three-dimensional room.

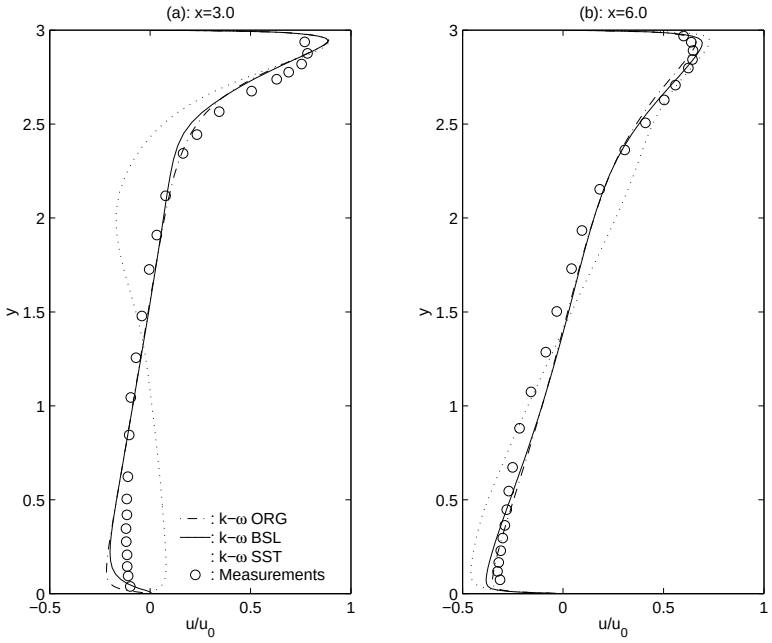

Figure 7.4: Dimensionless velocities $\frac{u}{u_0}$ along two vertical lines for the $k-\omega$ ORG, $k-\omega$ BSL and $k-\omega$ SST. Measurements along the same lines in the symmetry plane of the three-dimensional room.

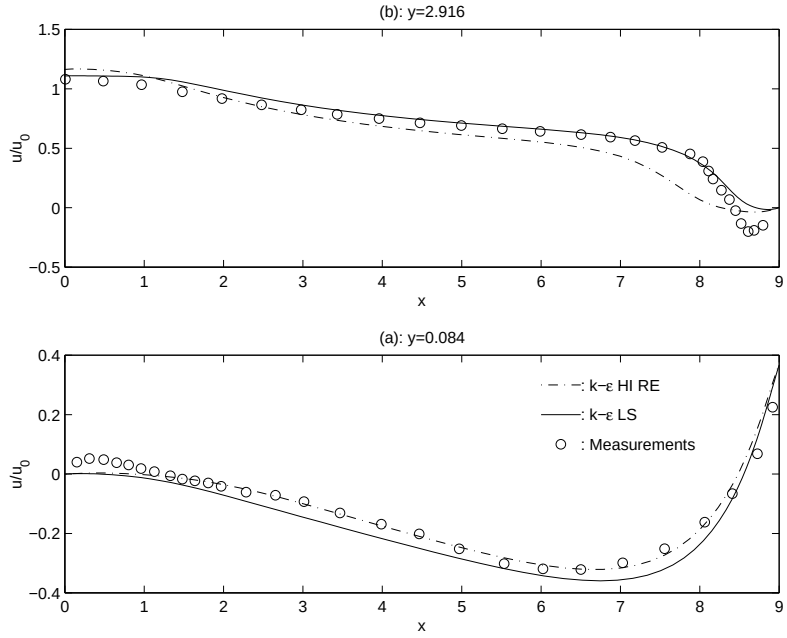

Figure 7.5: Dimensionless velocities $\frac{u}{u_0}$ along two horizontal lines for the $k-\epsilon$ HI RE and $k-\epsilon$ LS. Measurements along the same lines in the symmetry plane of the three-dimensional room.

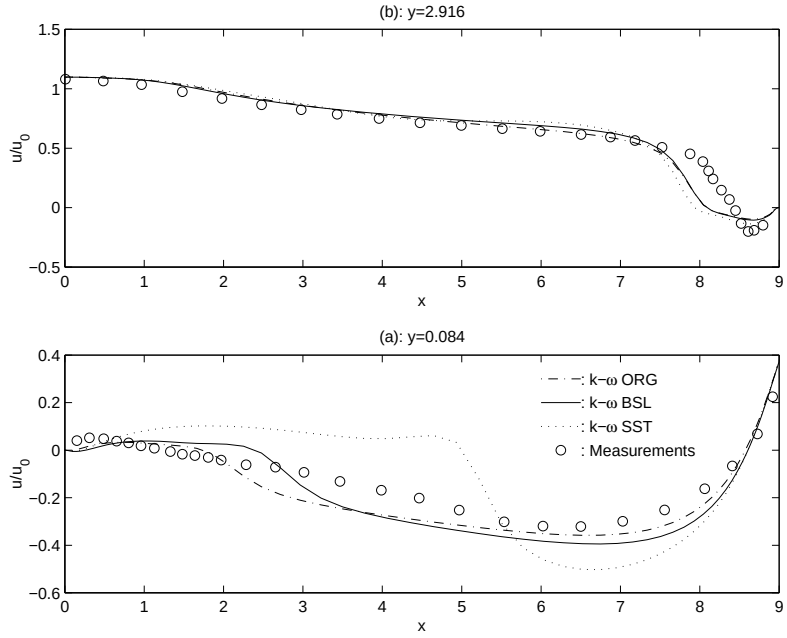

Figure 7.6: Dimensionless velocities $\frac{u}{u_0}$ along two horizontal lines for the $k-\omega$ ORG, $k-\omega$ BSL and $k-\omega$ SST. Measurements along the same lines in the symmetry plane of the three-dimensional room.

7.2 Comparing turbulent kinetic energy

The turbulent kinetic energy is an important quantity to assess the validity of the turbulence models. A comparison of this quantity is troublesome, since measurements are in one direction only.
According to [10], the correlation between the normal stresses in a two-dimensional wall jet is given by

$$\overline{u_2'^2} \approx 0.6\ \overline{u_1'^2} \quad \text{and} \quad \overline{y^2} \approx 0.8\ \ \overline{u_1'^2}. \tag{7.1}$$

We introduce (7.1) in the definition for the turbulent kinetic energy and thus

$$\sqrt{k} \approx 1.1\ \sqrt{\overline{u_1'^2}}. \tag{7.2}$$

If instead, we consider the flow as a boundary layer on a flat plate, a different correlation between the normal stresses is measured by Klebanoff, see Schlichting [15]. Using this correlation the factor 1.1 in (7.2) would take both higher and lower values throughout the boundary layer. In general only an increment of this constant would improve the agreement between computations and measurements, see figures 7.7-7.10. For simplicity we therefore use the relation (7.2).

In figure 7.7-7.10 calculated values of $\frac{\sqrt{k}}{1.1u_0}$ are compared with measurements of $\frac{\sqrt{\overline{u_1'^2}}}{u_0}$ for the various turbulence models. Except from the $k-\omega$ SST model, the models give almost similar distribution of the turbulent kinetic energy. The models tends to underpredict the turbulent kinetic energy, except in the wall jet, i.e. y between 2.5 and 3 in 7.7(a) and figure 7.8(a), and a small region close to $y = 1.5$. It is not clear whether the good accordance between measurements and computations in the wall jet should be ascribed (7.2) or the fact, that we are close to the supply opening in which the turbulence intensity is specified. The tendency for the used models to underpredict the turbulent kinetic energy is also reported by Schmidt [16] for the flow past a fence on a wall. We restrict ourselves to these conclusion due the uncertainty on the measurements. An interesting task for future studies is to carry out measurements in more than one direction. This would enable us to evaluate the expression (7.2) and conclude further on the performance of the turbulence models.

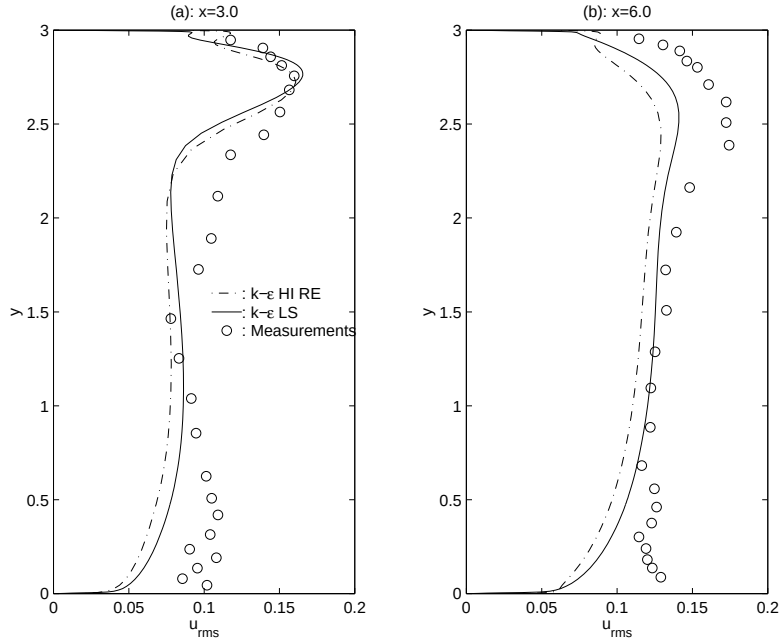

Figure 7.7: Turbulent kinetic energy $\frac{\sqrt{k}}{1.1u_o}$ along two vertical lines for the $k-\epsilon$ HI RE and $k-\epsilon$ LS. Measurements of $\frac{\sqrt{\overline{u_1'^2}}}{u_0}$ in the symmetry plane of the three dimensional room.

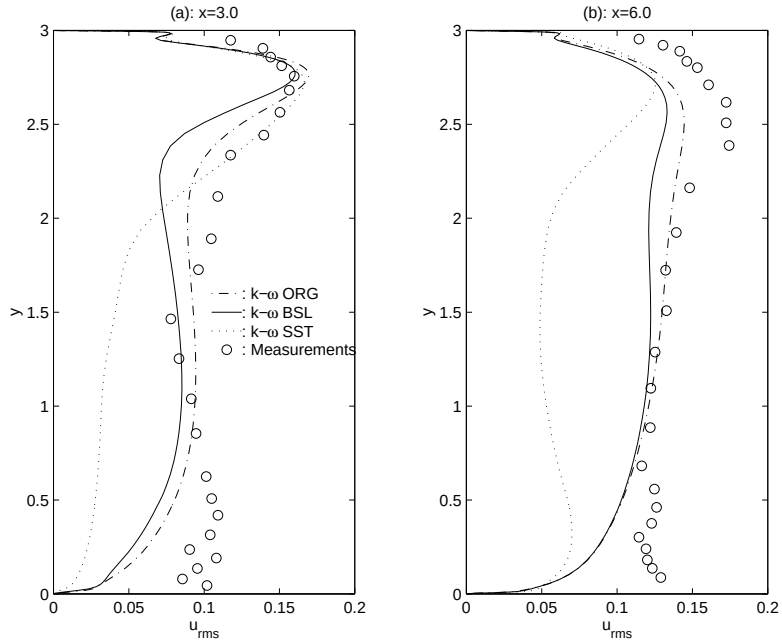

Figure 7.8: Turbulent kinetic energy $\frac{\sqrt{k}}{1.1u_o}$ along two vertical lines for the $k-\omega$ ORG, $k-\omega$ BSL and $k-\omega$ SST. Measurements of $\frac{\sqrt{\overline{u_1'^2}}}{u_0}$ in the symmetry plane of the three dimensional room.

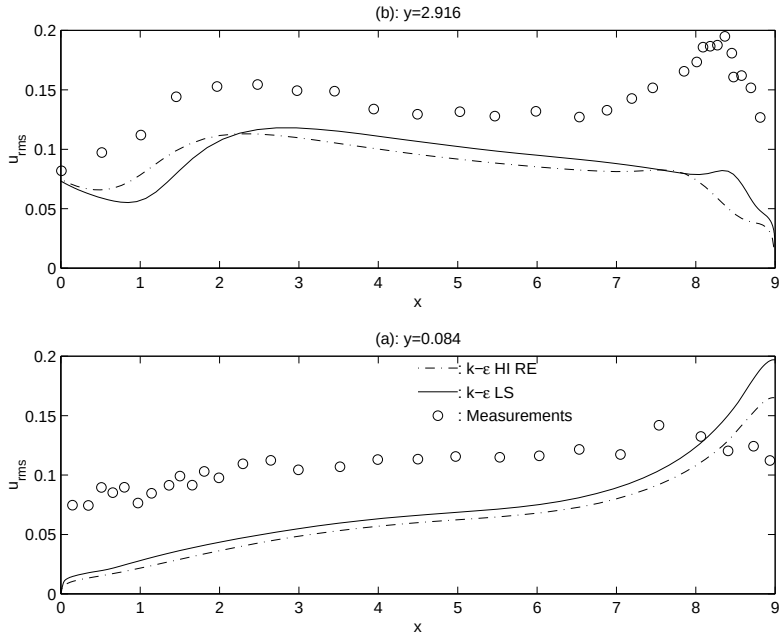

Figure 7.9: Turbulent kinetic energy $\frac{\sqrt{k}}{1.1u_o}$ along two horizontal lines for the $k-\epsilon$ HI RE and $k-\epsilon$ LS. Measurements of $\frac{\sqrt{\overline{u_1'^2}}}{u_0}$ in the symmetry plane of the three dimensional room.

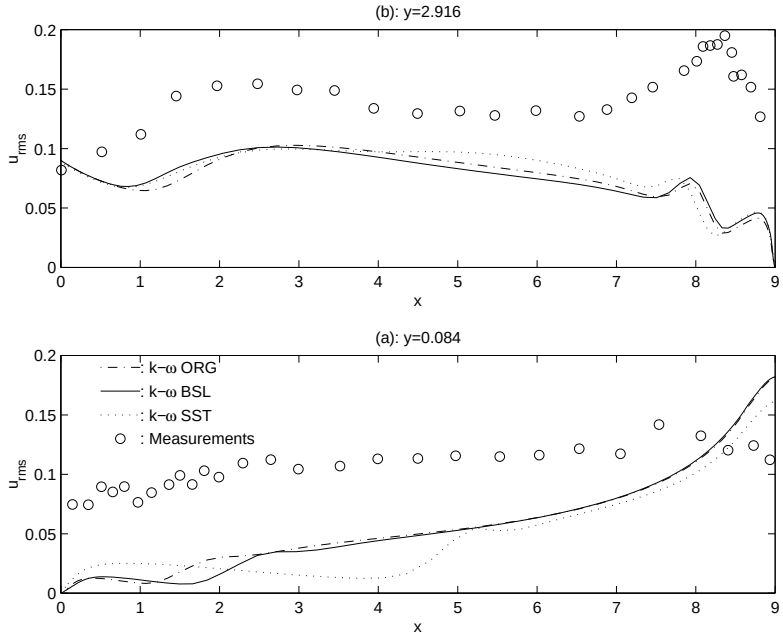

Figure 7.10: Turbulent kinetic energy $\frac{\sqrt{k}}{1.1u_o}$ along two horizontal lines for the $k-\omega$ ORG, $k-\omega$ BSL and $k-\omega$ SST. Measurements of $\frac{\sqrt{\overline{u_1'^2}}}{u_0}$ in the symmetry plane of the three dimensional room.

Chapter 8

Conclusion

In this report we have documented the ability of the flow solver *EllipSys2D* to give velocity distributions in good agreement with measurements for the annex 20 room.

A detailed presentation of the two-dimensional isothermal annex 20 testcase is given. Subsequently we use decomposition of the flow quantities for a rigorous derivation of the transport equations for the turbulent quantities k and ϵ. We briefly discuss near-wall asymptotic analysis, damping functions and boundary conditions, which are all interesting topics related to wall bounded flows. Furthermore, we describe in detail the five turbulence models chosen for testing. A method for hyperbolic netstretch is presented. Finally we discuss the solution procedure for the flow solver, before presenting the numerical results.

The numerical results achieved with the standard $k-\epsilon$ model, the low Reynolds number $k-\epsilon$ model by Launder & Sharma, the $k-\omega$ model by Wilcox, and the $k-\omega$ BSL model by Menter are almost equally good and leads to results in reasonably good agreement with measurements. Integrating the transport equations for k and ϵ to the walls instead of using wall laws has little to no effect on the numerical results, though the number of grid points needed to obtain a grid-independent solution are increased considerably. For the given flow it was impossible to both obtain a satisfying resolution of the wall jet and at the same time fulfill the requirement to the value of the sublayer scaled distance for the standard $k-\epsilon$ model. Therefore, for this kind of flow, these models should be used with caution. For the $k-\omega$ model by Wilcox and $k-\omega$ BSL model by Menter an extraordinary behaviour of the horizontal velocity component is found near the lower left corner. The four models mentioned above all show the same discrepancy between calculation and measurements close to $y = 1$ and $x = 6$. We have reason to believe, that this phenomenon is caused by three-dimensional effects.

Finally the $k-\omega$ SST model by Menter performed poorly. We believe that this is caused by the limiter added to the eddy viscosity, but it is not investigated further.

References

[1] Arpaci, V.S. & Larsen, P.S (1984) *Convection Heat Transfer.* Prentice-Hall, Inc. New Jersey, 2-63.

[2] Bradshaw, P., Ferriss, D.H. & Atwell, N.P. (1967) *Calculation of boundary-layer development using the turbulent enrgy equation.* Journal of Fluid Mechanics, vol. 28, part 3, 593-616.

[3] Launder, B.E. & Sharma, B.I. (1974) *Application of the Energy Dissipation Model of Turbulence to the Calculation of Flow Near a Spinning Disk.* Letters in Heat and Mass Transfer, Vol.1, No.2.

[4] Mansour, N.N., Kim, J., Moin, P., (1989) *Near-Wall $k-\epsilon$ Turbulence Modeling.* AIAA Journal, Vol.27, No.8, August, 1068-1073.

[5] Menter, F.R., (1993) *Zonal Two Equation $k-\omega$ Turbulence Models for Aerodynamical Flows.* AIAA Paper No93-2906, 24th Fluid Dynamics Conference, Florida, 1-21.

[6] Menter, F.R. (1994) *Two-Equation Eddy-Viscosity Turbulence Models for Engineering Applications.* AIAA Journal, Vol.32, No.8, August, 1598-1605.

[7] Michelsen, J.A., (1992) *Basis3D-a Platform for Development of Multiblock PDE Solvers.*, AFM 92-05, Department of Fluid Mechanics.

[8] Michelsen, J.A., (1989) *Solution of the Navier-Stokes equations on general non-orthogonal meshes.*, AFM 89-08, Department of Fluid Mechanics.

[9] Nielsen, P.V. (1990) *Specification of a Two-dimensional Test Case.*, International Energy Agency, Annex 20: Air Flow Pattern Within Buildings., Department of Building Technology and Structural Engineering, Åborg University, ISSN 0902-7513 R9040, 11-15.

[10] Nielsen, P.V. (1989) *Airflow Simulation Techniques - Progress and Trends.*, 10th AIVC Conference on Progress and Trends in Air Infiltration and Ventilation Research, vol.1, 203-223, ISBN o 946075 45x, The Air Infiltration and Ventilation Centre, Coventry

[11] Nielsen, P.V., Restivo, A. and Whitelaw, J.H. (1978) *The velocity Characteristics of Ventilated Rooms.*, Journal of FLuids Engineering, vol.100, September, 291-298.

[12] Patankar, S.V., (1980) *Numerical Heat Transfer and Fluid Flow.*, Hemisphere Publishing Corporation.

[13] Patankar, S.V. & Spalding, D.B., (1972) *A Calculation Procedure for Heat, Mass and Momentum Tranfer in Three-Dimensional Parabolic Flows.*, Int. Journal Heat and Mass Transfer, 15:1787.

[14] Rhie, C.M., (1981) *A numerical study of the flow past an isolated airfoil with separation.* Ph.D. thesis, University of Illinois, Urbane- Champaign.

[15] Schlichting, H., (1968) *Boundary-Layer Theory.* McGraw-Hill Book Company.

[16] Schmidt, Jens J., (1997) *Experimental and numerical investigation of separated flows.*, ET-PHD 97-01, Department of Energy Engineering, Fluid mechanics Section., 105-163.

[17] Speziale, C.G., Ridha, A., Anderson, E.C., (1992) *Critical Evaluation of Two-Equation Models for Near-Wall Turbulence.* AIAA Journal, Vol.30, No.2, February, 324-331.

[18] Sørensen, N.N., (1995) *General Purpose Flow Solver Applied to Flow over Hills.* Ph.D. Thesis, Risø National Laboratory, Roskilde, Denmark, Risø-R-827(EN).

[19] Sørensen, N.N., (1995) $k-\omega$ *Turbulence Models Implementation and Testing.* Risø National Laboratory, Roskilde, Denmark, Risø-R-864(EN).

[20] Tennekes, H & Lumley, J.L, (1972) *A First Course in Turbulence.* MIT Press Design Department.

[21] Wilcox, D.C., (1988) *Reassessment of the Scale-Determining Equation for Advanced Turbulence Models.* AIAA Journal, Vol.26, No.11, November, 1299-1310.

[22] Wilcox, D.C. (1993) *Turbulence Modeling for CFD.*, DCW Industries, Inc.

[23] Wilcox, D.C., (1993) *Comparison of Two-Equation Turbulence Models for Boundary Layers with Pressure Gradient.* AIAA Journal, Vol.31, No.8, August, 1414-1421.

Appendix A

Study on grid influence

A.1 Standard $k - \epsilon$ model

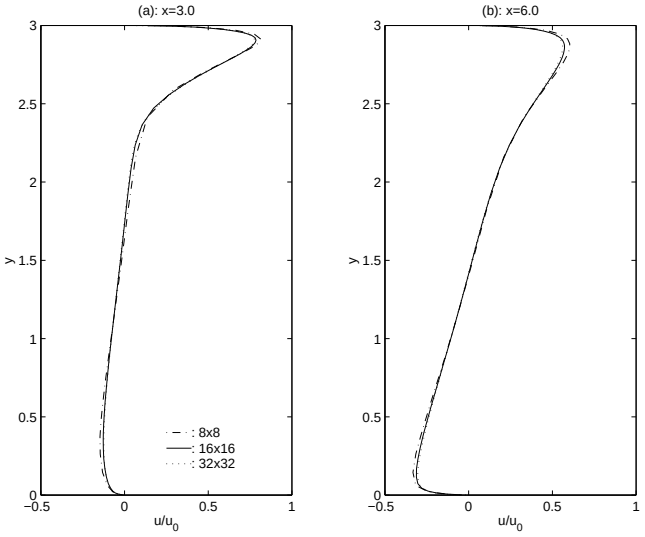

Figure A.1: Dimensionless horizontal velocities, $\frac{u}{u_0}$, along two vertical lines in the symmetryplane.

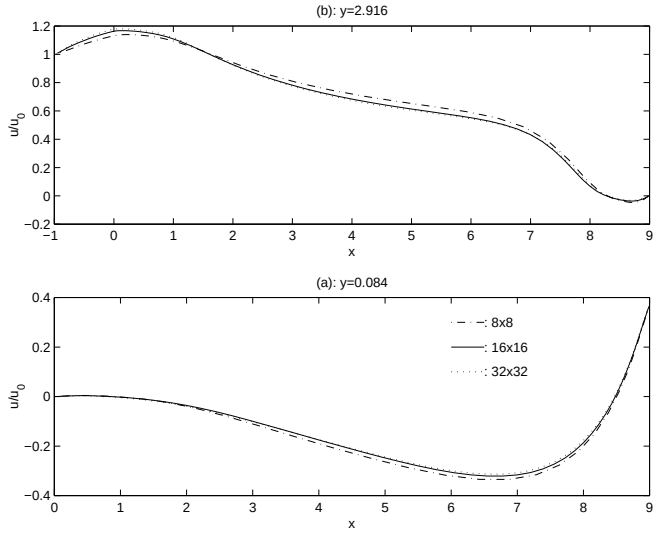

Figure A.2: Dimensionless horizontal velocities, $\frac{u}{u_0}$, along two horizontal lines in the symmetryplane.

A.2 Low Reynolds number $k - \epsilon$ model by Launder & Sharma

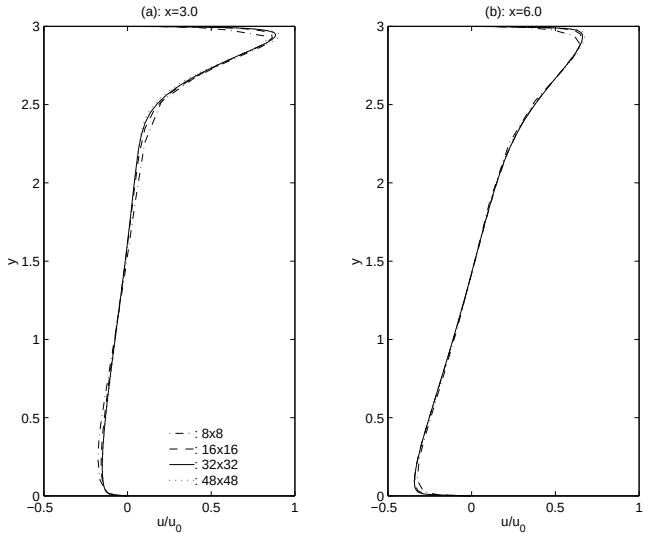

Figure A.3: Dimensionless horizontal velocities, $\frac{u}{u_0}$, along two vertical lines in the symmetryplane.

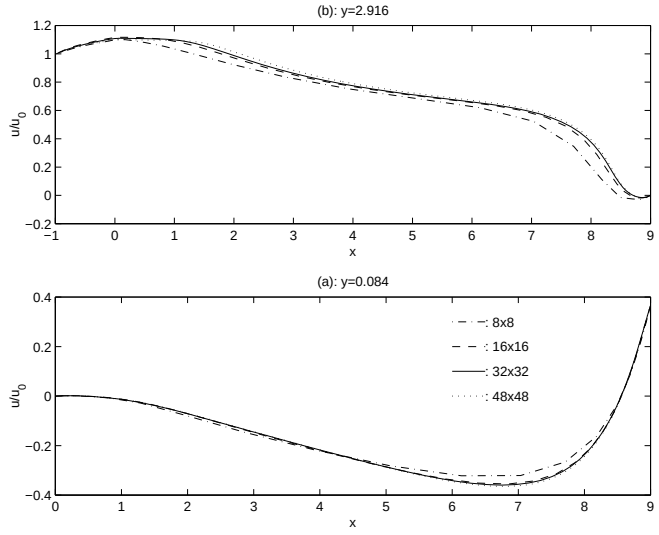

Figure A.4: Dimensionless horizontal velocities, $\frac{u}{u_0}$, along two horizontal lines in the symmetryplane.

A.3 $k-\omega$ model by Wilcox

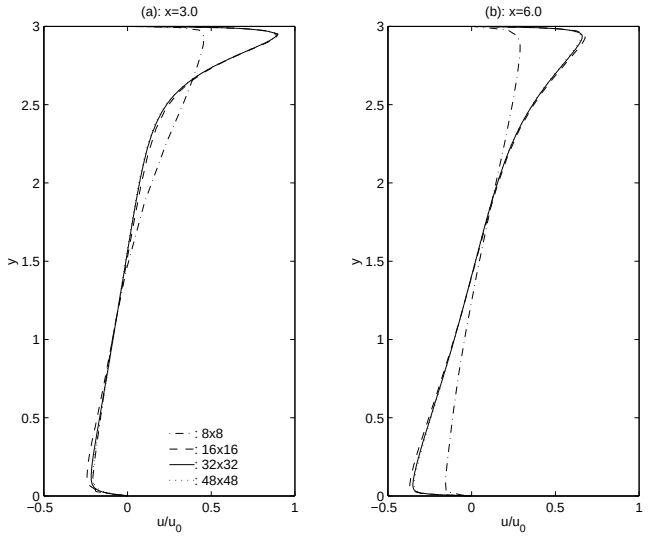

Figure A.5: Dimensionless horizontal velocities, $\frac{u}{u_0}$, along two vertical lines in the symmetryplane.

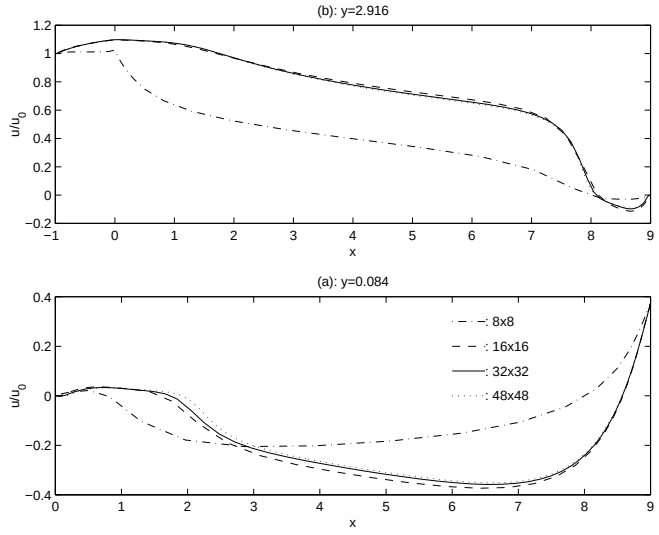

Figure A.6: Dimensionless horizontal velocities, $\frac{u}{u_0}$, along two horizontal lines in the symmetryplane.

A.4 $k-\omega$ BSL model by Menter

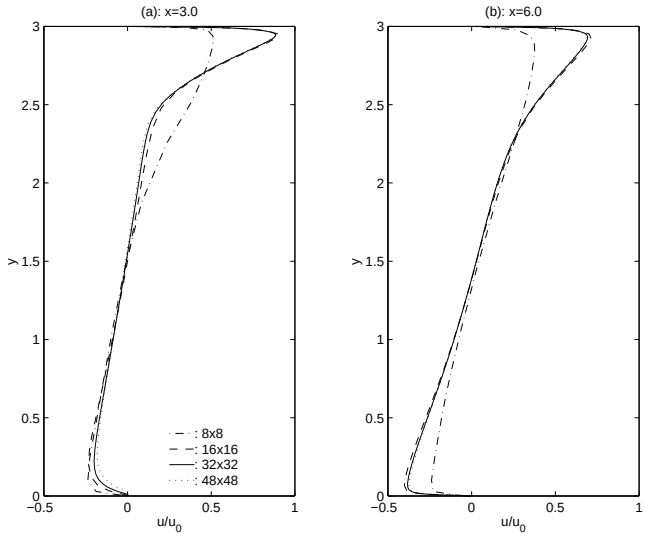

Figure A.7: Dimensionless horizontal velocities, $\frac{u}{u_0}$, along two vertical lines in the symmetryplane.

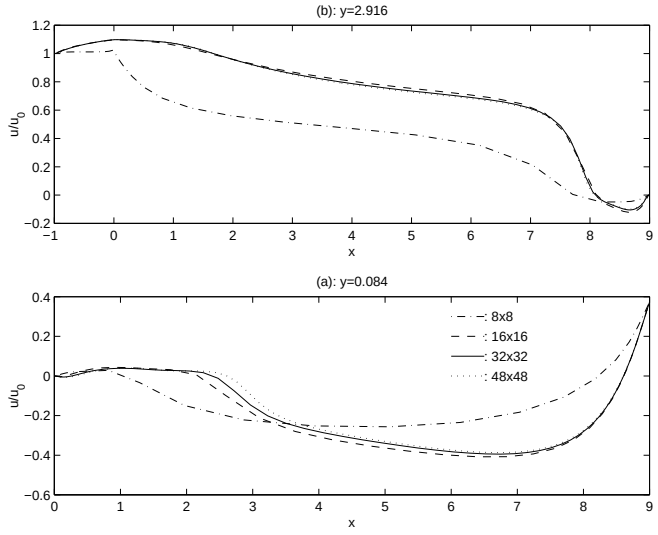

Figure A.8: Dimensionless horizontal velocities, $\frac{u}{u_0}$, along two horizontal lines in the symmetryplane.

A.5 $k-\omega$ SST model by Menter

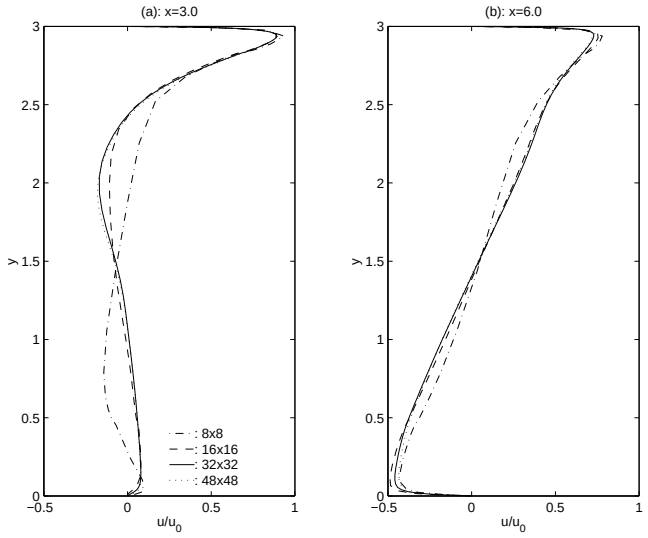

Figure A.9: Dimensionless horizontal velocities, $\frac{u}{u_0}$, along two vertical lines in the symmetryplane.

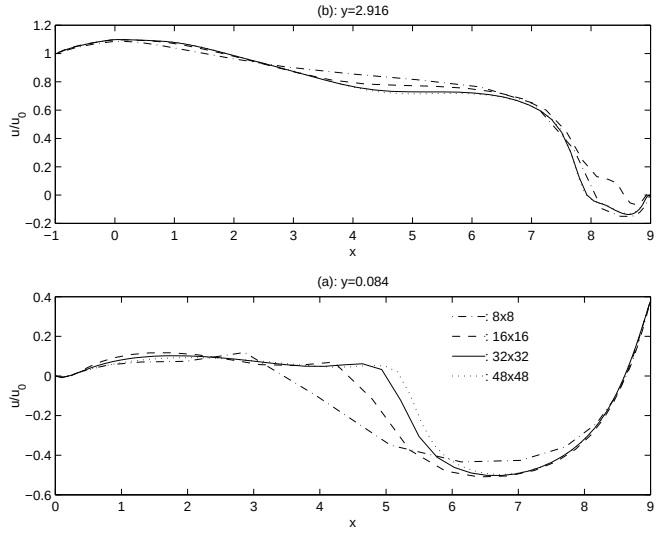

Figure A.10: Dimensionless horizontal velocities, $\frac{u}{u_0}$, along two horizontal lines in the symmetryplane.